A mouse forward genetics screen identifies LISTERIN as an E3 ubiquitin ligase involved in neurodegeneration

Jessie Chu[a,1], Nancy A. Hong[b,2], Claudio A. Masuda[c,3], Brian V. Jenkins[a], Keats A. Nelms[d], Christopher C. Goodnow[d], Richard J. Glynne[c], Hua Wu[b,4], Eliezer Masliah[e], Claudio A. P. Joazeiro[c,5], and Steve A. Kay[a,6,7]

[a]Department of Biochemistry, Institute for Childhood and Neglected Diseases, The Scripps Research Institute, ICND216, 10550 North Torrey Pines Road, La Jolla, CA 90237; [b]Phenomix Corporation, 5871 Oberlin Drive, Suite 200, San Diego, CA 92121; [c]Genomics Institute of the Novartis Research Foundation, 10675 John Jay Hopkins Drive, San Diego, CA 92121; [d]Phenomix Australia, Pty., Ltd., Level 3 Building 117, Australian Phenomics Facility, Garran Road, Acton, ACT 2601, Australia; and [e]Department of Neurosciences, University of California San Diego, School of Medicine, La Jolla, CA 92093

This contribution is part of the special series of Inaugural Articles by members of the National Academy of Sciences elected in 2008.

Contributed by Steve A. Kay, December 19, 2008 (sent for review November 13, 2008)

A mouse neurological mutant, *lister*, was identified through a genome-wide *N*-ethyl-*N*-nitrosourea (ENU) mutagenesis screen. Homozygous *lister* mice exhibit profound early-onset and progressive neurological and motor dysfunction. *lister* encodes a RING finger protein, LISTERIN, which functions as an E3 ubiquitin ligase in vitro. Although *lister* is widely expressed in all tissues, motor and sensory neurons and neuronal processes in the brainstem and spinal cord are primarily affected in the mutant. Pathological signs include gliosis, dystrophic neurites, vacuolated mitochondria, and accumulation of soluble hyperphosphorylated tau. Analysis with a different *lister* allele generated through targeted gene trap insertion reveals LISTERIN is required for embryonic development and confirms that direct perturbation of a LISTERIN-regulated process causes neurodegeneration. The *lister* mouse uncovers a pathway involved in neurodegeneration and may serves as a model for understanding the molecular mechanisms underlying human neurodegenerative disorders.

Neurodegenerative disorders are a group of diseases with distinct etiology and molecular bases. These diseases predominately occur as sporadic cases, and the causes are complex and multifactorial. Nevertheless, causative mutations for some cases of neurodegenerative disorders, such as Alzheimer's disease (AD), Amyotrophic Lateral Sclerosis (ALS) and Parkinson's disease (PD) have been identified. Importantly, some of the linked genes are also involved prominently in the pathology of sporadic forms of these diseases. For example, mutation in α-synuclein results in early onset familial PD (1), and α-synuclein is a major component of Lewy bodies and of Lewy neuritic pathology in both familial PD and sporadic PD (1–4). Identification of causative genes for neurodegenerative disorders also allows the development of genetic mouse models that are valuable tools for providing insights into the pathogenesis and molecular pathways leading to degeneration.

To date, the genetic or molecular basis of the majority of neurological disorders remains largely undetermined (5–7). For example, Cu/Zn Superoxide dismutase (SOD1) mutations account for only ≈2% of all ALS patients (6). To identify other causal genes or risk factors involved in neurodegeneration, we performed a forward genetic screen, using ENU-mediated random mutagenesis. ENU is a powerful DNA alkylating agent in mouse spermatogonial germ cells. Because ENU primarily induces DNA point mutations that can result in partial loss- or gain-of-function phenotypes that predominate in human diseases (8), this strategy for identifying mouse disease models is potentially more productive for modeling human neurodegenerative disorders than traditional gene-targeting approaches in mice. Indeed, this approach has generated many models of human disease. For example, mutation in Myo7a induced by ENU generated a rat model for human Usher syndrome type 1B (9). Further, ENU-induced mutation in dynein led to progressive motor neuron degeneration in mice (10). Although no human disease has yet been mapped to dynein itself, mutation in the dynein activator, dynactin, causes degeneration of lower motor neurons in humans (11). Thus, the ENU dynein model correctly predicted that errors in a particular machinery would give rise to human disease.

Here, we report the identification and characterization of a mutant mouse model of neurodegeneration, and cloning of the affected gene, *lister*. Histological analysis of *lister* mutants shows several pathological biomarkers seen in human neurodegenerative diseases. The *lister* mouse uncovers a pathway involved in neurodegeneration and may serves as a model for understanding the molecular mechanisms underlying human neurodegenerative disorders.

Results

Through ENU mutagenesis screening, we have identified a recessive mutation that manifests as a progressive movement disorder. Newborn homozygous mutants are found with the expected Mendelian ratio, and although initially show no significant differences in general appearance or body weight, these animals exhibit age-dependent and often asymmetrical progressive weakness of hind limbs, bradykinesia and eventually loss of locomotor ability (Movie S1). Because of the "tilting" or "listing" phenotype, we have named the mutant "*lister*." One of the earliest neurological symptoms apparent in homozygous *lister* mice is the loss of hind limb extension reflex, which is charac-

Author contributions: J.C., N.A.H., C.A.M., C.A.P.J., and S.A.K. designed research; J.C., C.A.M., B.V.J., and H.W. performed research; K.A.N., C.C.G., R.J.G., and E.M. contributed new reagents/analytic tools; J.C., N.A.H., C.A.M., B.V.J., and S.A.K. analyzed data; and J.C., N.A.H., C.A.P.J., and S.A.K. wrote the paper.

The authors declare no conflict of interest.

[1]Present address: La Jolla Laboratories, Pfizer Inc, 10646 Science Center Drive, San Diego, CA 92121.

[2]Present address: Forward Ventures, 9393 Towne Centre Drive, Suite 200, San Diego, CA 92121.

[3]Present address: Instituto de Bioquímica Médica, Programa de Biologia Molecular e Biotecnologia, Universidade Federal do Rio de Janeiro, 21941–590, Rio de Janeiro, Brazil.

[4]Present address: Novartis Institute for Biomedical Research, Inc., Cambridge, MA 02139.

[5]Present address: Department of Cell Biology, CB168, The Scripps Research Institute, 10550 North Torrey Pines Road, La Jolla, CA 90237.

[6]Present address: Division of Biological Science, UCSD, 9500 Gilman Drive, La Jolla, CA 92093.

[7]To whom correspondence should be addressed. E-mail: skay@ucsd.edu.

This article contains supporting information online at www.pnas.org/cgi/content/full/0812819106/DCSupplemental.

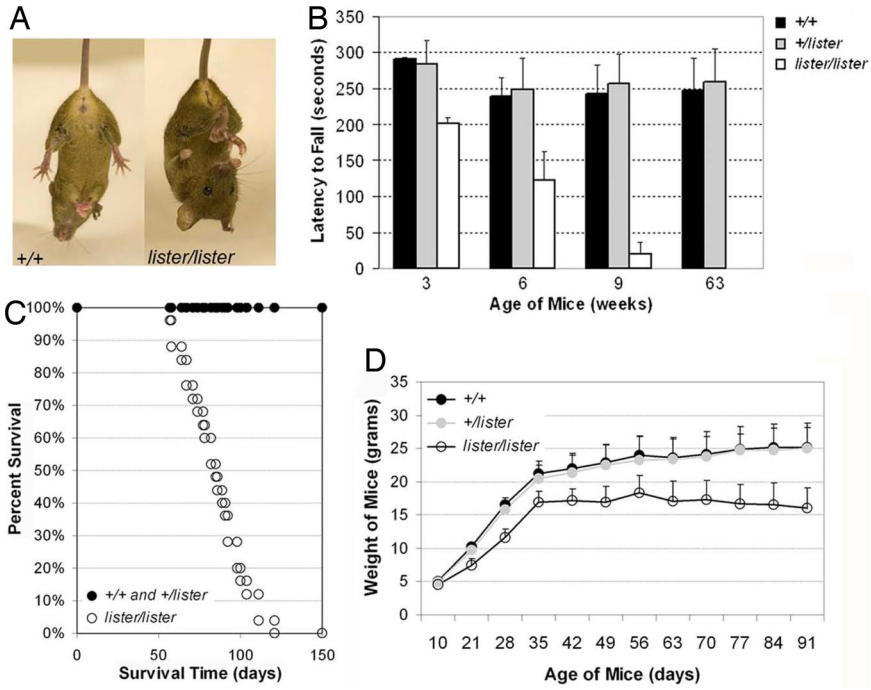

Fig. 1. Progressive impairment of neuronal and motor functions associated with weight loss and reduced life span in *lister* mutant mice. (*A*) Loss of hind limb extension reflex in *lister/lister* mutant manifested by hind limb clenching when lifted by the tail. (*B*) Motor function of *lister/lister* mutants (white bars, $n = 8$) compared with heterozygous (gray bars, $n = 12$) and wild-type littermates (black bars, $n = 12$) measured by accelerated rotarod test. +/+ versus *lister/lister* mice: $P < 0.0005$ at 3 weeks of age, $P < 0.02$ at 6 weeks of age, $P < 0.0005$ at 9 weeks of age. *lister*/+ ($n = 12$) versus +/+ mice ($n = 10$): $P = 0.127$ at 63 weeks of age. (*C*) Survival curve of homozygous *lister* mutants (white circles, $n = 25$) compared with heterozygous and wild-type littermates (black circles, $n = 25$). (*D*) Body weight curve for +/+ (black circles, $n = 14$), *lister*/+ (gray circles, $n = 32$) and *lister/lister* mice (white circles, $n = 14$).

terized by spasmodic grasping movements and flexing of the hind limbs (Fig. 1*A*). The onset and progression of the symptoms varies among individual animals but consistently worsens over time when compared with age-matched wild-type or heterozygous animals (Fig. S1*A*). Balance and motor coordination were tested by an accelerating rotarod paradigm. *lister/lister* mice have markedly reduced performance by 3 weeks of age, the earliest time at which a reliable behavioral assessment could be performed. Heterozygotes remain indistinguishable from wild-type mice for up to a year (Fig. 1*B*). The progression of motor deficits was also monitored by a righting reflex test (Fig. S1*B*) and grip strength test (data not shown). In combination, these assays demonstrate an age-dependent decrease in motor function of *lister* homozygotes that progresses until a terminal stage generally between 2 to 3 months of age (Fig. 1*C*). There is no clear gender effect with respect to onset of symptoms or lifespan (data not shown). Starting at ≈3 weeks of age, *lister/lister* mice appear smaller in size compared with wild-type or heterozygous littermates. Homozygous animals show reduced growth rate and eventual weight loss over time (Fig. 1*D*). Reduction of weight could be due to loss of muscle mass secondary to motor dysfunction and/or to insufficient food intake resulting from facial motor weakness driven by impairment of brainstem lower motor neurons (see below). It is possible that the mutation may cause direct effects on growth potential as well. Together, these phenotypes are consistent with impairment in the central nervous system (CNS), such as basal ganglia, brainstem, cerebellum or spinal cord.

Consistent with motor impairment of *lister* homozygotes, histological analyses detected several neuropathological signs after the progression of the disease in the CNS. Routine hematoxylin and eosin (H&E) staining and immunohistochemical analysis for glial fibrillary acidic protein (GFAP) revealed reactive astrogliosis in midbrain, brainstem and spinal cord starting from intermediate stage (≈6 weeks of age) (Fig. S2 *A–C*). Mild astrogliosis is also seen in thalamus and hypothalamus (data not shown). Along the spinal cord, GFAP-reactive astrocytes are first detected in the ventral horn and intermediate zone of lumbar sections, and then found in the thoracic and cervical sections as disease progresses, indicating neuronal injury in these areas (Fig. 2 *A* and *B*). Gallyas silver staining revealed dystrophic neurites in *lister/lister* brainstems and spinal cords (Fig. 2 *C* and *D*). These silver-positive structures occur after phenotype onset and increase in density as disease progresses. Another neuropathology observed in both brain and spinal cord of symptomatic homozygous *lister* mice are hyperphosphorylated forms of the microtubule-associated protein, tau, as recognized by phosphorylation-specific antibodies AT-8 and AT-180 (Fig. 2*E Left*). Both phospho-antibody reactivity and protein migration were altered upon treatment with phosphatase (Fig. 2*E Right*). Abnormal phosphorylation of tau disrupts its affinity for microtubules and affects its contribution to maintaining axon integrity, which may provoke neurodegeneration (12). However, unlike the insoluble aggregates observed in AD patients, and in brains from certain AD mouse models (13), the hyperphosphorylated tau in *lister* mice remains soluble in sarkosyl buffer (Fig. 2*F*). This is similar to the increase of soluble hyperphosphorylated tau in the SOD1 (G37R) transgenic ALS model (14). This observation is consistent with the idea that soluble, prefibrillar forms of hyperphosphorylated tau can be neurotoxic (15, 16).

To look closer at the morphology of dystrophic neuronal processes and neurons in symptomatic *lister* homozygotes, we used Transmission Electron Microscopy (TEM) to examine the ultrastructures of cells and neuropil in the anterior horn of lumbar region of spinal cord. Electron-dense dying neurons are observed in *lister* homozygous but not wild-type animals (Fig. S3 *A* and *B*). Consistent with the Gallyas silver positive deposits in

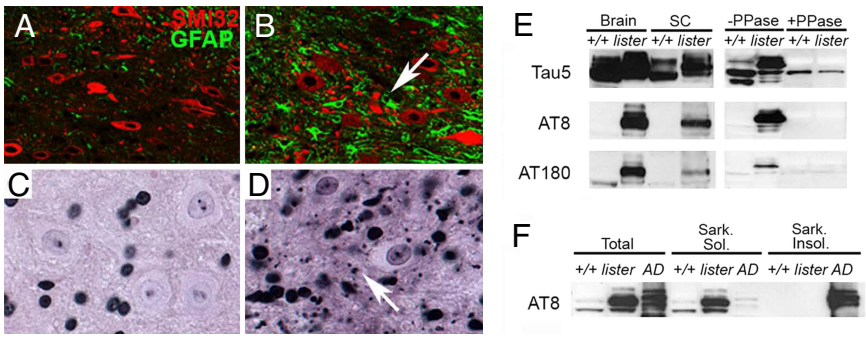

Fig. 2. Increased astrogliosis, dystrophic neurites, and accumulation of soluble hyperphosphorylated tau in *lister* mutant mice. Histopathological analysis of the CNS of wild-type (*A* and *C*) and *lister/lister* mice (*B* and *D*). (*A* and *B*) GFAP (green) staining of wild-type and *lister/lister* ventral horn sections of spinal cord; reactive astrogliosis is highlighted (arrow) in *B*. SMI32 (red) recognizes nonphosphorylated NF-H. (*C* and *D*) Gallyas silver staining of wild-type and *lister/lister* spinal cords. The arrow indicates a silver-positive dystrophic neurite. (*E*) Western blots of brain and spinal cord extracts from *lister/lister* and aged matched +/+ mice using both phosphorylation-dependent (AT-8 and AT-180) and -independent (TAU-5) tau antibodies. Western blots of brain extract after phosphatase treatment of immunoprecipitated tau using TAU-5 from wild-type and *lister/lister* mice (*Right*). (*F*) Distribution of hyperphosphorylated tau within soluble and insoluble fractions obtained by sarkosyl extraction of *lister/lister* mice and AD brain cortex.

the gray matter, abnormal and degenerating axons are found scattering in the gray matter and the white matter (Fig. S3 *B*, *D*, and *F*). In addition, although most presynaptic profiles and synapses appear normal in *lister* mutants, postsynaptic profiles often appear swollen with vacuolated mitochondria compared with wild-type animals (Fig. S3 *E* and *F*). Pronounced vacuolated mitochondria phenotypes observed in *lister* mutants are similar to the ones observed in transgenic mice with G93A mutant SOD1 (17). Taken together, these morphological changes of the mitochondria and pathological signatures in spinal cord and brainstem correlate with clinical features in lower motor neuron (LMN) diseases, whereas the morphology of Gallyas positive pathological lesions resemble argyrophilic grains in degenerative tauopathies (18). Therefore, the *lister* mouse models pathological hallmarks of different human neurological disorders.

Because *lister* mice show motor dysfunction, and since pathological markers are evident in the brainstem and spinal cord, we looked for evidence of motor neuron degeneration. In the lumbar region of the spinal cord, we observed reduction of large diameter (>25 μm) motor neurons in terminal-stage *lister* mutants but not in younger mice (Fig. 3*G*). We did not detect apoptosis by either TUNEL assay or immunohistochemistry, using an antibody to detect activated caspase 3 (data not shown), although TEM revealed dying neurons. Most of the dying neurons have undergone a shrinkage process as indicated below. In addition, toluidine blue staining reveals scattered degenerative axons in the lateral and ventral side of the spinal cord white matter of symptomatic mice (Fig. 3 *A* and *B*). To quantify the progression of degenerative motor neurons, the number and diameter of axons were measured from the L5 roots collected at different disease stages. Both motor and sensory axons are of normal number and size at symptom onset (3 weeks of age) (Fig. 3*H* and Fig. S4 *A* and *B*). As disease progresses, axonal degeneration in both motor and sensory roots is observed. In the motor roots the number of total axons is reduced, and axons of larger caliber size preferentially degenerated (Fig. 3 *H* and *I*). In addition, the number of intermediate-size axons increased, indicating that some of the larger caliber axons underwent shrinkage. Predominant loss of large axonal fibers is a typical sign of ALS (19). As with motor axons, there is also loss of sensory axons in the *lister* mice, and the remaining axons are of smaller caliber (Fig. 3 *H* and *J*). Despite severe motor dysfunction in *lister* mice, the reduction of motor axons from the L5 root was not as significant as seen in SOD1 mouse model (20). We therefore asked whether distal axons showed signs of degeneration. Upon examination of the femoral nerve longitudinally we found that although the proximal end appeared to be morphologically normal, some of the distal ends were severely degenerated (Fig. 3 *C* and *D* and Fig. S4 *B* and *C*). Detailed analysis by TEM revealed unraveled myelin together with axoplasm that had collapsed or shrunk to a very modest level in many of the fibers (Fig. 3 *C* and *D*). This indicates the axons degenerate through a dying-back process. In addition, the number of proximal axons may not reflect the functionality of these axons and likely underestimates disease status in *lister* mice. Consistent with motor axonal destruction, muscle atrophy, smaller muscle fiber size and isolated regeneration of muscle fibers were found in the hind limb muscles (Fig. 3 *E* and *F*). These data suggest that motor neurons' abnormal dendrites and degenerating axons lead to cell death or shrinkage, and likely contribute to motor dysfunction in *lister* mice. Thus, these mice exhibit a bona fide neurodegenerative disorder sharing many common pathological features of human diseases.

To map the *lister* mutation, *lister* heterozygous C57BL/6 (B6) mice were out-crossed to wild-type NOD.B10BR H-2^k congenic mice, and resultant progeny were intercrossed. Genomic DNA samples from affected N1F1 mice were genotyped with a panel of >200 SNPs. The mutation was further localized through fine mapping to a 3.6-Mb interval on mouse chromosome 16 between (and excluding) genes encoding β-amyloid precursor protein (APP) and SOD1 (Fig. 4 *A* and *B*). A set of 27 keratin- and keratin-associated protein-related genes were not considered likely to be associated with the *lister* phenotype, whereas there were at least 5 genes with evidence for expression in the nervous system, making them candidates for the *lister* gene. Direct genomic DNA sequencing covering splice sites and exons of 10 non-keratin related genes identified an A-T transversion at a splice donor site in a gene of unknown function (ENSMUSG00000052299) (Fig. 4*C*). The resulting transcript has an internal deletion of exon 11, but the original reading frame of the protein is preserved, resulting in expression of a mutant protein product lacking the 14 aa encoded by exon 11 (Fig. 4*D*). Mis-spliced transcript and mutant protein were detected in vivo (Fig. 4*E*). Expression of the mutant protein was decreased in late-stage, symptomatic *lister* animals (Fig. 4*F*). Although the LISTERIN antibodies do not work for immunohistochemistry, in situ hybridization shows that *lister* is broadly expressed within the CNS (Fig. S5*A*); in addition, *lister* mRNA transcripts are found in all tissues examined (21). Histological analysis found no pathological signs in major organs of *lister* homozygotes, and no abnormal cell death or cell proliferation in tissues outside the nervous system (data not shown).

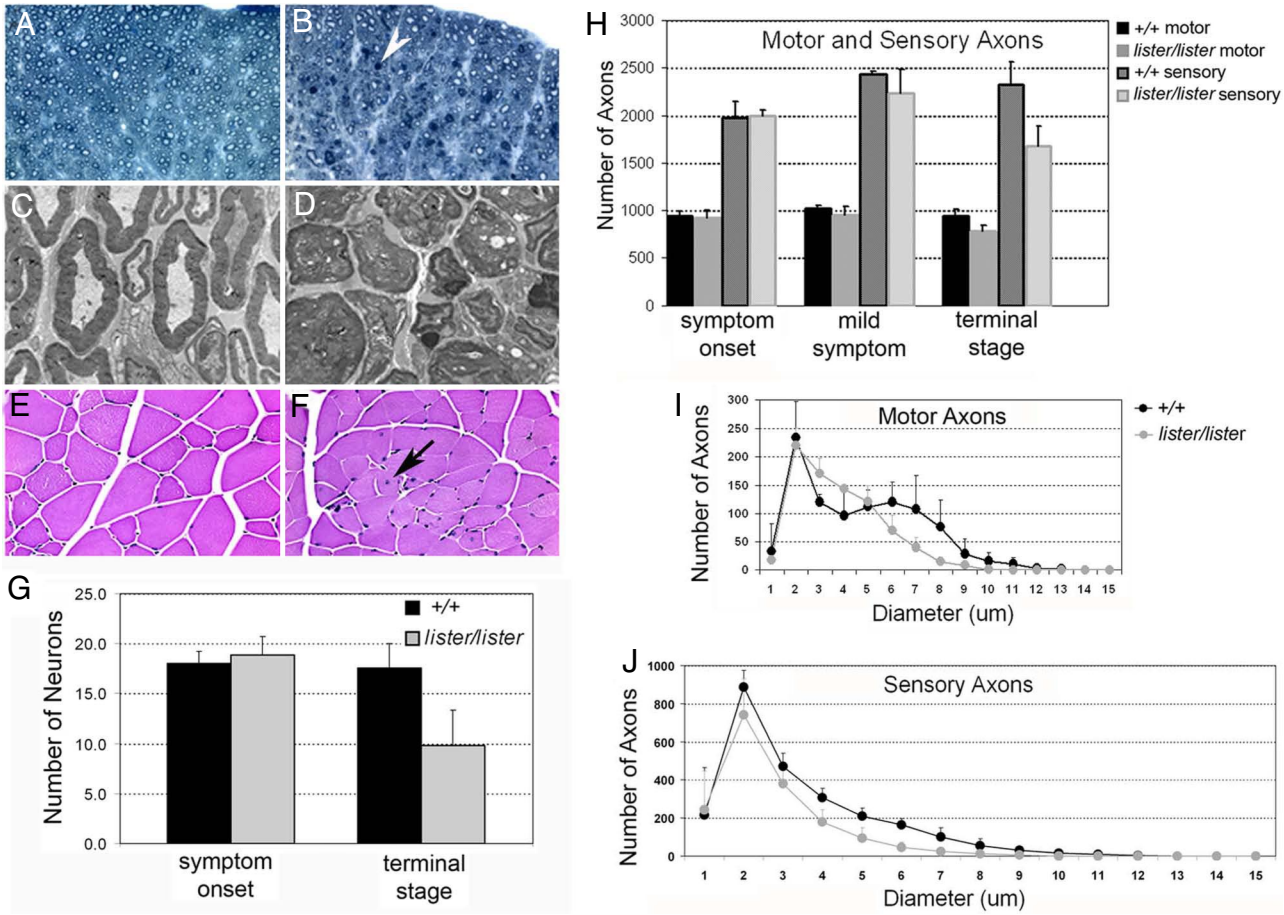

Fig. 3. Axonal and neuronal degeneration and muscle pathology in *lister* mutant mice. (*A* and *B*) Toluidine blue staining of white matter of spinal cord from wild-type and *lister/lister*, respectively. Arrowhead indicates a degenerating axon. (*C* and *D*) TEM images of distal femoral nerve branches of wild-type and *lister* mutants, respectively. (*E* and *F*) H&E staining of hind-leg quadriceps skeletal muscles from wild-type and *lister/lister* animals, respectively. Arrow indicates a centrally nucleated muscle fiber. (*G*) Comparison of number of motor neurons >25 μm in diameter in lumbar spinal cord between +/+ (black bars, $n = 5$) and *lister/lister* (gray bars, $n = 7$) mice at symptom onset ($P = 0.639$) and terminal stage ($P < 0.05$). (*H*) Number of axons counted from cross sections of motor and sensory L5 roots in *lister/lister* and wild-type littermates at different stages ($n = 3$–5 each genotype per age group). +/+ versus *lister/lister* mice at symptom onset for motor root ($P = 0.741$) and sensory root ($P = 0.135$), at terminal stage for motor root ($P < 0.05$) and sensory root ($P < 0.01$). (*I* and *J*) Distribution of axon diameters from the entire motor and sensory roots of terminal-staged *lister/lister* (gray circles) versus +/+ (black circles).

The LISTERIN protein contains a conserved lysine-rich domain at the amino terminus and a conserved RING finger at the carboxyl-terminus (Fig. 4 *G* and *H*). Because most RING finger containing proteins function as E3 ubiquitin ligases (22, 23), this suggests that LISTERIN may be involved in ubiquitylation of cellular substrates. Ubiquitylation is a multistep post-translational modification that occurs via the sequential action of at least 3 classes of enzymes, the ubiquitin-activating (E1), ubiquitin-conjugating (E2) and ubiquitin-ligase (E3) (24). E3 ligases recognize the target protein and hence dictate the high specificity of the reaction (24). RING finger E3s interact with ubiquitin-bound E2s (via the RING finger) and with substrates (usually via other domains in the polypeptide) and mediate ubiquitin transfer to a Lysine residue of the target protein (22). To test whether or not the RING domain of LISTERIN has E3 activity in vitro, ubiquitylation assays containing ubiquitin, E1, E2 (Ubc4), and a GST fusion with the LISTERIN RING finger were performed. Western blot analysis of the reaction products revealed autoubiquitylation derivatives of the GST-RING, in a reaction that required all components (Fig. 4*I*). Thus, the LISTERIN RING finger has intrinsic E3 activity in vitro. Because the 14-aa deletion in mutant LISTERIN is distal to the RING finger, we expect the mutant protein to be active in E2 binding and in promoting ubiquitin transfer in vivo (Indeed, both wild-type and mutant full length LISTERIN show similar ubiquitylation activity in vitro; data not show). However, the 14-aa deletion may affect substrate binding, the orientation of the RING finger relative to the substrate, or lead to defective substrate ubiquitylation by some other mechanism. The identification of relevant substrates will allow these hypotheses to be tested directly.

The neurodegenerative phenotype of *lister/lister* homozygotes could conceivably be due to a separate ENU-induced mutation in a tightly linked gene. To test this possibility, we generated mice carrying a gene trap allele of *lister*. The ß-geo gene trap ES cell line *RRR322* has an insertion site in intron 25 of *lister*. The resulting transcript is a fusion of exons 1–25 of *lister* and the ß-geo gene leading to the production of truncated LISTERIN lacking the RING finger domain (Fig. S6*A*). Heterozygous *RRR322* mice are asymptomatic and homozygous *RRR322* mice are embryonic lethal for reasons still under investigation. This suggests that LISTERIN RING domain is essential for normal embryonic development and that the ENU mutation does not lead to a complete abolishment of LISTERIN ubiquitylation function, and is most likely a hypomorphic allele. The lethality of the homozygous *RRR322* mice generated by gene targeting

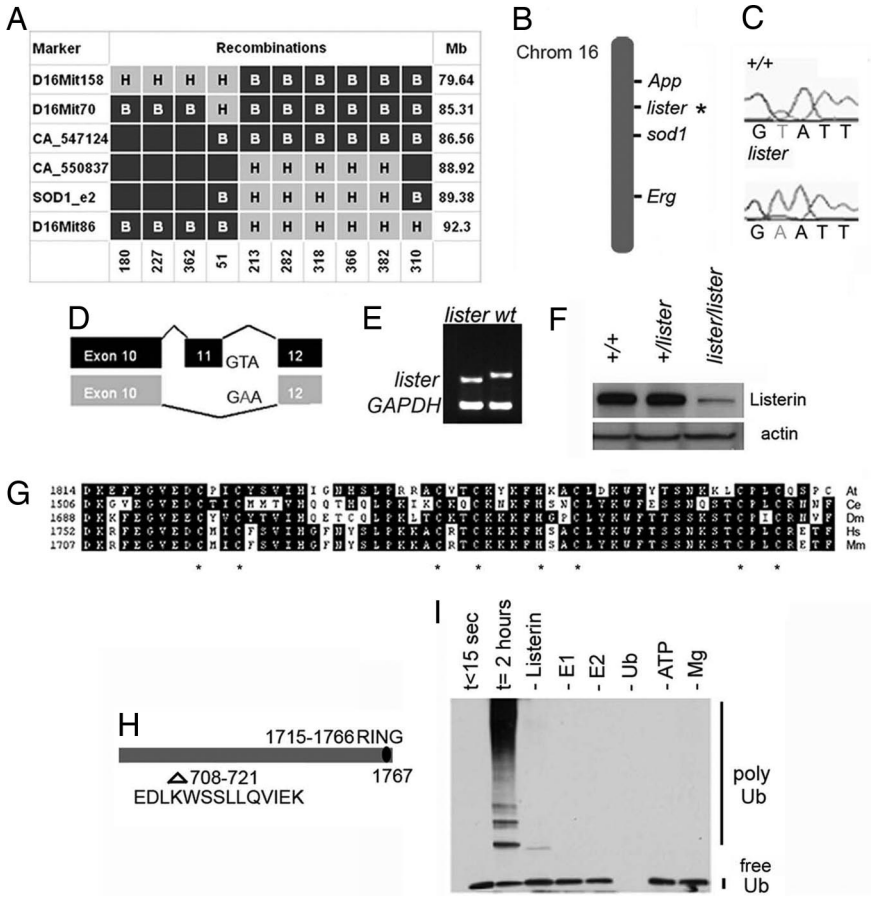

Fig. 4. Molecular and biochemical characterization of *lister* transcript and LISTERIN protein. (*A*) Haplotype mapping of the *lister* interval on chromosome 16. All recombinant mice shown are affected. Black squares labeled ''B'' denote B6 homozygotes, gray squares labeled ''H'' denote B6;NOD, H-2k heterozygotes, and unlabeled squares are inferred. All physical positions are relative to the National Center for Biotechnology Information Build 34 mouse genome assembly. (*B*) The *lister* gene on the mouse chromosome 16. (*C*) T → A transversion in *lister* gene. (*D*) The mutation results in removal of a splice-donor site in *lister* and an internal deletion of exon 11, while the original reading frame is preserved. (*E*) Detection of altered mRNA splicing in *lister* mutant by RT-PCR. (*F*) Western blot of LISTERIN expression in mouse spinal cord extracts from terminal-stage *lister*/*lister* and +/+ mice. (*G*) Alignment of mouse LISTERIN RING domain and its homologs. The asterisk highlights the conserved zinc-chelating residues in the RING domain. At, *Arabidopsis thaliana*; Ce, *C. elegance*; Dm, *Drosophila melanogaster*; Hs, *Human sapien*; Mm, *Mus musculus*. (*H*) LISTERIN primary structure with a conserved RING finger at its C terminus and the location of the deleted 14 aa in the *lister* allele. (*I*) Products of in vitro ubiquitylation assay in a drop-out experiment using the LISTERIN RING finger, revealed by Western blot with anti-ubiquitin antibody.

approach highlighted a major advantage of the ENU-based mutagenesis approach, which is to induce informative hypomorphic alleles that result in partial loss of gene function and interesting adult phenotypes. Importantly, *lister*/*RRR322* compound heterozygotes developed the hind limb clasping phenotype and progressive movement deficits (Fig. S6*B* and Movie S2), and have reduced weight and shortened survival similar to that of *lister*/*lister* homozygotes (data not shown). This strongly suggests that the neurological phenotypes observed in *lister*/*lister* mice are due to disrupted function of the LISTERIN protein. One cannot yet rule out the possibility that ENU mutated LISTERIN has aberrant activity that can somehow be masked by a wild-type copy of LISTERIN. However, because the LISTERIN product of the *lister* allele has an intact RING finger, which exhibits E3 activity, whereas LISTERIN of the *RRR322* allele lacks the RING finger, the simplest explanation for the similarity of the *lister*/*lister* and *lister*/*RRR322* phenotypes is that both are due to defective substrate ubiquitylation, which over time could lead to neuronal dysfunction and degeneration.

Discussion

Here, we report the identification of a RING finger E3 ligase, LISTERIN, involved in neurodegeneration. The *lister* phenotype is similar to a variety of human neurodegenerative disorders in that, whereas the causative gene product is expressed widely, selective neuronal cell types, including sensory and motor neurons, are particularly vulnerable (25). We note that, because *lister* is expressed ubiquitously, one cannot rule out that the source of toxicity does not initiate from the affected neurons themselves. For example, motor neuron cell death in SOD1 mutant mice is not cell autonomous and depends upon surrounding cells (26–28).

lister mice can be used as a model for studying sensory-motor axonal neuropathy, spinal-bulbar muscular atrophy (SBMA), or ALS. Although classic ALS is considered a motor neuron specific disease, there may be more widespread degeneration with time (29). Indeed, in addition to motor neuron degeneration, sensory neuropathy is found associated with SBMA (30), and some autosomal-dominant juvenile ALS cases (31). There is also good evidence indicating significant overlap between ALS and FTD (32). Linkage mapping and genome-wide association will determine whether *lister* may be a causal gene or a susceptibility gene for human neurological disease. Alternatively, *lister* mutations in humans may predispose or affect disease onset and progression to neurodegeneration caused by other factors.

Motor and sensory neurons degenerate in a ''dying-back'' fashion in *lister* mutants as in other mouse models. However, the

L5 axonal loss occurs late in disease. This is different from motor neuron degeneration in SOD1 mouse model where L5 axonal degeneration occurs at symptom onset (20). Thus, although axonal degeneration may contribute to clinical symptoms of *lister* mice, it is likely not the primary cause of the motor dysfunction phenotype. A pathological sign that precedes L5 axonal loss is the observation of dystrophic neuritis and abnormal dendrites with vacuolated mitochondria in the spinal cord. The motor deficits observed in *lister* mice may thus result from synaptic dysfunction and loss of connectivity.

LISTERIN is required for normal development, as demonstrated by the embryonic lethality of *RRR322* homozygous mice. Moreover, *lister* mice show a detectable phenotype as early as within 3 weeks of age (the earliest time point that we conducted quantitative behavioral analysis). It is therefore possible that neurodegeneration results, in part, from the impairment of LISTERIN-dependent regulation of neuronal development. Such effects, although initially subtle, would eventually become sufficient to affect neuronal viability. Further study of the developmental function of LISTERIN should lead to better understanding of the critical role of LISTERIN for neuronal survival.

The ubiquitin-proteasome system (UPS) is a critical regulator of numerous cellular processes. In the nervous system, ubiquitylation is also a major determinant of neuronal-specific mechanisms, such as synaptic function. Not surprisingly, defects in the ubiquitin system, affecting either general protein quality control or specific processes or pathways, contribute to the pathophysiology of neurodegenerative diseases: (*i*) The failure to degrade mutant or misfolded proteins can lead to aggregate formation and disease (33). (*ii*) Mutations directly affecting enzymes of the ubiquitin conjugation/deconjugation pathway have been identified in human neurodevelopmental and neurodegenerative disorders. This includes *UBE3A*, encoding the E6-AP E3 ubiquitin ligase mutated in Angelman syndrome (34, 35), Parkin, an E3 ubiquitin ligase mutated in juvenile recessive and familial PD (36), and ubiquitin carboxyl-terminal hydrolase-L1 (UCH-L1) in PD (37). (*iii*) Neurodegeneration has also been described as a result of mutation of UPS components in mice, such as in the RING E3 Mahogunin (Mgrn1) (38) and in the deubiquitylating enzyme *Usp14* (39).

The above findings suggest that impairment of ubiquitin-regulated processes is often sufficient to cause a wide spectrum of neuronal disorders. However, exactly how defects in UPS components lead to specific neurodegenerative phenotypes remains unknown. The identification of LISTERIN as a new component of the ubiquitin system implicated in neurodegeneration thus provides a new and valuable resource to uncover genes and biochemical pathways disrupted in neurodegeneration and to potentially help elucidate general molecular mechanisms underlying these pathologies.

Materials and Methods

ENU Mutagenesis and Mapping. ENU mutagenesis was generated as described in ref. 40. In a library bred from ENU-treated C57BL/6 mice, a G3 male offspring developed paralysis at 4 months of age. A mutant breeding line (*lister*) was established by backcrossing this founder to normal C57BL/6 mice. Adult-onset paralysis was inherited as a single recessive Mendelian trait. To identify the *lister* mutation, B6 *lister* animals were outcrossed to wild-type NOD.B10BR H-2^k congenic mice. Affected N1F1 mice were genotyped with a panel of >200 SNPs on the Sequenom MassARRAY platform to reveal linkage to distal chromosome 16. The recombinational breakpoints in these animals were further delimited using simple sequence length polymorphism (SSLP) MIT markers between D16Mit25 and D16Mit86, positioning the *lister* mutation within a 7-Mb region between D16Mit70 and D16Mit86. SSLPs were identified using Ensembl repeat annotations to further narrow the region containing the *lister* mutation to a 3.6-Mb region that was predicted to contain exons from 39 genes. Direct genomic DNA sequencing covering splice sites and exons of 10 non-keratin related genes identified a single base change in the splice donor sequence following exon 11 of the *lister* gene, where a T → A transversion was discovered at the exon 11 splice junction. For genotyping *lister* mice, using the Sequenom MassARRAY system, primers used were: 5′capture primer: ACGTTGGATGAAGAAAGGGAAAGGGGAGAG 3′ capture primer: ACGTTGGATGTTTCAGGAGGACCTGAAGTG. Extend primer: CTTCAGGTCATTGAAAAGG.

Phenotypic and Behavioral Analysis. Mouse weight was measured at 10 days of age and every week afterward until terminal stage (see below). Accelerated Rotarod: Mice were put on the rotarod for practice 5 min before each session. For each session, 3 trials were performed with a resting interval of 5 min. The speed was accelerated from 4- 40 rpm in 5 min. Results are given as the duration mice were able to maintain their balance on the rod. The performance is the mean of 3 trials. Mice that rotated with the rod 2 full circles were considered as falling. Results were analyzed using Student's *t* test. Hind limb extension reflex: Mice were suspended by the tail for 30 seconds and the severity of the clasping phenotype was quantified by the time required to exhibit clenching (0 = no clenching in 30 sec, 1 = clenching in 21–30 sec, 2 = clenching in 11–20 sec, 3 = clenching in 6–10 sec, 4 = clenching in 5 sec, 5 = clenching in 5 sec and difficulty in recovering). Righting reflex: Mice were placed in the supine position, and the time to regain upright posture was recorded. Mice that failed to right themselves within 1 min were considered terminal stage. The animals' care was in accordance with institutional guidelines.

Tissue Preparation, Histology, and Immunohistochemistry and in Situ Hybridization. Heavily anesthetized mice were perfused intracardially with 4% paraformaldehyde in 0.1M Sorensen's phosphate buffer, pH 7.2, and postfixed overnight in the same buffer. Paraffin sections were stained with H&E, Nissl or Gallyas stain. Immunohistochemical staining was performed on deparaffinized sections and treated with antigen unmasking solution according to manufacturer's protocol (Vector Laboratories). Sections were blocked in 1% BSA, 0.2% fat free milk, 5% normal goat serum in PBS, pH 7.4, for 1 h at room temperature. Primary antibodies were incubated in blocking solution overnight at 4 °C. Primary antibodies used were rabbit anti-GFAP (Dako) at 1:500 dilution and mouse anti-nonphosphoneurofilament SMI32 (Sternberger Monoclonals Inc.) at 1:1,000. Secondary antibodies were Alexa Fluor 488 goat anti-mouse and Alexa Fluor 568 goat anti-rabbit (Molecular Probes) at 1:1,000 for 1 h at room temperature. In cases where biotin-conjugated anti-rabbit secondary antibodies were used, samples were processed using Vector ABC kit according to the manufacturer's protocol (Vector Laboratories). Motor neuron scoring: Nissl-stained spinal cord sections were collected and imaged. Cells with nuclei visible and diameter >25 μm in ventral horn region were counted. For each animal, sections were analyzed every 30 μm, for 20 sections, n = 5–7 each genotype per age group. Results were analyzed using Student's' *t* test. In situ hybridization: Adult tissues were dissected, fixed in 4% paraformaldehyde in PBS, cryoprotected in 30% sucrose, and frozen in OCT mounting medium in dry ice with 90% ethanol. Cryostat sections (5–7 μm) were processed and hybridized with a digoxygenin RNA probe generated by in vitro transcription (Roche) from a cDNA encoding LISTERIN. The specific mouse *lister* mRNA antisense riboprobe correspond to nucleotide 2265–3121of the *lister* cDNA sequence (NCBI accession no. XM_128374). PCR products were amplified from mouse brain cDNA library, using the following primers: GGACTTGGAAGCCACAACAT and TGTCGAGTTCTTCACACCAC. Fluorescence detection was carried out with the Tyramide Signal Amplification kit (NEN Life Sciences).

Axon Preparation and Morphological Analysis. L5 axons were prepared and analyzed as described in ref. 41, with the following modifications. Samples were embedded in Technovit 7100 according to manufacturer's protocol (Heraeus). Cross-sectional area and numbers of axons were analyzed using MetaMorph imaging software (Molecular Devices). The cross-sectional area of each axon was calculated and reported as a diameter of a circle of equivalent area. Axon diameters were grouped into 1-μm bins.

Transmission Electron Microscopy. After being anesthetized, mice were perfused intracardially with 4% paraformaldehyde, 1.5% glutaraldehyde in 0.1M Na cacodylate buffer and after exposure of the spinal cord and femoral nerves, fixation was continued overnight in situ at 4 °C. The relevant tissues were dissected and fixed in 3% glutaraldehyde in 0.1M cacodylate buffer, then buffer washed, postfixed in 1% osmium tetroxide and subsequently dehydrated in a graded ethanol series followed by propylene oxide. The tissue pieces were embedded in EMbed 812/Araldite (Electron Microscopy Sciences). Sixty-nanometer-thin transverse sections were cut, mounted on copper slot grids coated with parlodion and stained with uranyl acetate and lead citrate.

Protein Extraction and Western Blot Analyses. Mouse brain and spinal cord were homogenized and sonicated in lysis buffer [50 mM Tris·HCl pH 8.0, 150 mM NaCl, 0.5% Nonidet P-40, 0.5% DOC, 0.5% SDS, 5 mM EDTA, 5 mM NaF, 1 mM Na3VO4 and 1× Complete protease inhibitor mixture (Roche)]. Cell lysates were centrifuged at 21,000 × *g* at 4 °C for 15 min and the supernatants were collected. For sarkosyl soluble and insoluble fractions, mouse brain and spinal cord were homogenized in lysis buffer [10 mM Tris·HCl (pH 7.4), 0.8M NaCl, 1 mM EGTA, 1 mM EDTA, 10% sucrose, 5 mM NaF, 1 mM Na3VO4, 10 mM β-glycerophosphate and 1× complete protease inhibitors mixture (Roche)]. Cell lysates were centrifuged at 20,000 × *g* at 4 °C for 20 min and the supernatants were collected. Sarkosyl was added to the supernatant to a final concentration of 1% (vol/vol) and the samples were rocked for 1 h at room temperature. The samples were centrifuged at 100,000 × *g* at 4°C for 1 h. Supernatants (sarkosyl soluble fraction) were collected and the pellets (sarkosyl insoluble fraction) resuspended in 50 mM Tris·Cl (pH 7.4) in the same volume of the supernatants. Samples were stored at −80 °C until use. To examine the phosphorylation state of the microtubule associated protein tau, this protein was immunoprecipitated from ≈100 μg of brain and spinal cord extracts using the mouse anti-tau-5 antibody. After immunoprecipitation, half of the sample was stored on ice whereas the other half was treated with 20 units of calf intestinal alkaline phosphatase (USB) for 4 h at 37 °C. Proteins were separated by SDS/PAGE on 4–20% Tris-Glycine gradient gels (Invitrogen), and transferred onto nitrocellulose paper. Blots were blocked in 5% milk in TBST for 1 h. Primary bodies used: mouse anti-tau-5 at 1 μg/ml (Biosource), mouse anti-human PHF-tau, clone AT8 and AT180 (Autogenbioclear). A monoclonal Lister antibody (clone5L11) raised against a N-terminally truncated version of human LISTERIN (starting from N713) was used at 1:100. Secondary HRP-conjugated, goat anti-mouse antibody (Sigma; catalog no. A2554) was used at 1:10,000 and ECL-plus (G&E Biosciences) was used for detection (Pierce). Lysates from cortex from a patient (AD5150) with AD was prepared as described above. The sample was obtained from the Alzheimer Disease Research Center at the University of California, San Diego.

In Vitro Ubiquitylation Assay. DNA fragments encoding the RING domain of LISTERIN were subcloned by PCR with primers 5′-GGAAGTATCATGGAAGGCTT and 5′-TCAGAAAAGGTCTLACGGC into pGEX-4T2. GST-fusion proteins were produced in *E. coli* BL21(DE3) in TB with 100 μM ZnOAc and induced with 1 mM IPTG for 4 h at 30 °C. Cells were lysed in 50 mM Tris·HCl (pH 8), 120 mM NaCl, 1 mM DTT, and 1x complete protease inhibitors (Roche). Proteins bound to glutathione-Sepharose beads (Amersham Biosciences) were eluted with lysis buffer containing 20 mM glutathione and dialyzed against lysis buffer containing 20 mM Tris, pH 8 and100 mM NaCl with 5 mM β-ME (2-Mercaptoethanol) overnight. Ubiquitylation assay was performed as described in ref. 42.

Generation of RRR322 Mice. The RRR322 embryonic stem cell line was obtained from National Institutes of Health-sponsored NHLBI-BayGenomics and the NCRR-MMRRC. Chimeric mice were generated by the Mouse Genetics Core of The Scripps Research Institute (TSRI) according to standard procedures. The agouti offspring were tested for transmission of the disrupted allele by PCR. PCR primers used for genotyping the wild-type allele were 5′-TGCAGTGTGGATTGAACCAT and 5′-GTTGGTTTGCGGCTTTATGT, and the primers used for genotyping the RRR322 insertion allele were 5′-TGCAGTGTGGATTGAACCAT and 5′-CGACGGGATCCTCTAGAGTC.

ACKNOWLEDGMENTS. We thank L. Foster for early observations of the phenotype; D. Trajkovic (TSRI) for histology assistance; M.R. Woods (TSRI) for TEM; TSRI mouse genetic core for mouse line generation; C. Lee for LISTERIN expression; S. Cohen (Genomics Institute of the Novartis Research Foundation) for LISTERIN mAb generation, and M. Leissring and D.A. Figlewicz for comments on the manuscript. This work was supported by an Office Depot Grant (to S.A.K.), a Ruth L. Kirschstein National Institutes of Health Postdoctoral Fellowship (to J.C.), postdoctoral fellowships from the PEW Latin American Fellows Program in the Biomedical Sciences and from Conselho Nacional de Desenvolvimento Cientifico e Tecnologico (Brazil) (to C.A.M.), and American Cancer Society Research Scholar Grant 08-298-01-TBE (to C.A.P.J.). This is manuscript no. 18196-CB of The Scripps Research Institute

1. Singleton AB, *et al.* (2003) Alpha-Synuclein locus triplication causes Parkinson's disease. *Science* 302:841.
2. Spillantini MG, *et al.* (1997) Alpha-synuclein in Lewy bodies. *Nature* 388:839–840.
3. Kruger R, *et al.* (1998) Ala30Pro mutation in the gene encoding alpha-synuclein in Parkinson's disease. *Nat Genet* 18:106–108.
4. Zarranz JJ, *et al.* (2004) The new mutation, E46K, of alpha-synuclein causes Parkinson and Lewy body dementia. *Ann Neurol* 55:164–173.
5. Farrer MJ (2006) Genetics of Parkinson disease: Paradigm shifts and future prospects. *Nat Rev Genet* 7:306–318.
6. Figlewicz DA, Orrell RW (2003) The genetics of motor neuron diseases. *Amyotroph Lateral Scler Other Motor Neuron Disord* 4:225–231.
7. Hardy J, Orr H (2006) The genetics of neurodegenerative diseases. *J Neurochem* 97:1690–1699.
8. Nolan PM, Hugill A, Cox RD (2002) ENU mutagenesis in the mouse: Application to human genetic disease. *Brief Funct Genomic Proteomic* 1:278–289.
9. Smits BM, *et al.* (2005) Identification of a rat model for usher syndrome type 1B by N-ethyl-N-nitrosourea mutagenesis-driven forward genetics. *Genetics* 170:1887–1896.
10. Hafezparast M, *et al.* (2003) Mutations in dynein link motor neuron degeneration to defects in retrograde transport. *Science* 300:808–812.
11. Puls I, *et al.* (2003) Mutant dynactin in motor neuron disease. *Nat Genet* 33:455–456.
12. Cairns NJ, Lee VM, Trojanowski JQ (2004) The cytoskeleton in neurodegenerative diseases. *J Pathol* 204:438–449.
13. Buee L, Bussiere T, Buee-Scherrer V, Delacourte A, Hof PR (2000) Tau protein isoforms, phosphorylation and role in neurodegenerative disorders. *Brain Res Brain Res Rev* 33:95–130.
14. Farah CA, Nguyen MD, Julien JP, Leclerc N (2003) Altered levels and distribution of microtubule-associated proteins before disease onset in a mouse model of amyotrophic lateral sclerosis. *J Neurochem* 84:77–86.
15. Wittmann CW, *et al.* (2001) Tauopathy in Drosophila: Neurodegeneration without neurofibrillary tangles. *Science* 293:711–714.
16. Duff K, Planel E (2005) Untangling memory deficits. *Nat Med* 11:826–827.
17. Sasaki S, Warita H, Murakami T, Abe K, Iwata M (2004) Ultrastructural study of mitochondria in the spinal cord of transgenic mice with a G93A mutant SOD1 gene. *Acta Neuropathol* 107:461–474.
18. Tolnay M, Clavaquera F (2004) Argyrophilic grain disease: A late-onset dementia with distinctive features among tauopathies. *Neuropathology* 24:269–283.
19. Sobue G, Hashizume Y, Mitsuma T, Takahashi A (1987) Size-dependent myelinated fiber loss in the corticospinal tract in Shy-Drager syndrome and amyotrophic lateral sclerosis. *Neurology 3* 7:529–532.
20. Zhang B, Tu P, Abtahian F, Trojanowski JQ, Lee VM (1997) Neurofilaments and orthograde transport are reduced in ventral root axons of transgenic mice that express human SOD1 with a G93A mutation. *J Cell Biol* 139:1307–1315.
21. Su AI, *et al.* (2002) Large-scale analysis of the human and mouse transcriptomes. *Proc Natl Acad Sci USA* 99:4465–4470.
22. Joazeiro CA, Weissman AM (2000) RING finger proteins: Mediators of ubiquitin ligase activity. *Cell* 102:549–552.
23. Deshaies R, Joazeiro CA (2009) RING domain E3 ubiquitin ligases. *Annu Rev Biochem* 78. *in press.*
24. Hershko A, Ciechanover A, Varshavsky A (2000) Basic Medical Research Award. The ubiquitin system. *Nat Med* 6:1073–1081.
25. Green SL, Tolwani RJ (1999) Animal models for motor neuron disease. *Lab Anim Sci* 49:480–487.
26. Pramatarova A, Laganiere J, Roussel J, Brisebois K, Rouleau GA (2001) Neuron-specific expression of mutant superoxide dismutase 1 in transgenic mice does not lead to motor impairment. *J Neurosci* 21:3369–3374.
27. Lino MM, Schneider C, Caroni P (2002) Accumulation of SOD1 mutants in postnatal motoneurons does not cause motoneuron pathology or motoneuron disease. *J Neurosci* 22:4825–4832.
28. Clement AM, *et al.* (2003) Wild-type nonneuronal cells extend survival of SOD1 mutant motor neurons in ALS mice. *Science* 302:113–117.
29. Hand CK, Rouleau GA (2002) Familial amyotrophic lateral sclerosis. *Muscle Nerve* 25:135–159.
30. Li M, *et al.* (1995) Primary sensory neurons in X-linked recessive bulbospinal neuropathy: Histopathology and androgen receptor gene expression. *Muscle Nerve* 18:301–308.
31. Rabin BA, *et al.* (1999) Autosomal dominant juvenile amyotrophic lateral sclerosis. *Brain* 122:1539–1550.
32. Murphy J, Henry R, Lomen-Hoerth C (2007) Establishing subtypes of the continuum of frontal lobe impairment in amyotrophic lateral sclerosis. *Arch Neurol* 64:330–334.
33. Berke SJ, Paulson HL (2003) Protein aggregation and the ubiquitin proteasome pathway: Gaining the UPPer hand on neurodegeneration. *Curr Opin Genet Dev* 13:253–261.
34. Kishino T, Lalande M, Wagstaff J (1997) UBE3A/E6-AP mutations cause Angelman syndrome. *Nat Genet* 15:70–73.
35. Matsuura T, *et al.* (1997) De novo truncating mutations in E6-AP ubiquitin-protein ligase gene (UBE3A) in Angelman syndrome. *Nat Genet* 15:74–77.
36. Dawson TM, Dawson VL (2003) Molecular pathways of neurodegeneration in Parkinson's disease. *Science* 302:819–822.
37. Leroy E, *et al.* (1998) The ubiquitin pathway in Parkinson's disease. *Nature* 395:451–452.
38. He L, *et al.* (2003) Spongiform degeneration in mahoganoid mutant mice. *Science* 299:710–712.
39. Wilson SM, *et al.* (2002) Synaptic defects in ataxia mice result from a mutation in Usp14, encoding a ubiquitin-specific protease. *Nat Genet* 32:420–425.
40. Jun JE, *et al.* (2003) Identifying the MAGUK protein Carma-1 as a central regulator of humoral immune responses and atopy by genome-wide mouse mutagenesis. *Immunity* 18:751–762.
41. Garcia ML, *et al.* (2003) NF-M is an essential target for the myelin-directed ''outside-in'' signaling cascade that mediates radial axonal growth. *J Cell Biol* 163:1011–1020.
42. Joazeiro CA, *et al.* (1999) The tyrosine kinase negative regulator c-Cbl as a RING-type, E2-dependent ubiquitin-protein ligase. *Science* 286:309–312.